Supporting Information

Oxidation State and Surface Reconstruction of Cu under CO_2 Reduction Conditions from *In Situ* X-ray Characterization

Soo Hong Lee[1,2,‖], John C. Lin[3,4,‖], Maryam Farmand[1,2], Alan T. Landers[4,5], Jeremy T. Feaster[3,4], Jaime E. Avilés Acosta[4,6], Jeffrey W. Beeman[1,2], Yifan Ye[1,2,7], Junko Yano[1,8], Apurva Mehta*[,9], Ryan C. Davis*[,9], Thomas F. Jaramillo*[,3,4], Christopher Hahn*[,4], and Walter S. Drisdell*[,1,2]

[1]*Joint Center for Artificial Photosynthesis and* [2]*Chemical Sciences Division, Lawrence Berkeley National Laboratory, 1 Cyclotron Rd., Berkeley, CA 94720, United States*

[3]*Department of Chemical Engineering, Stanford University, Stanford, CA 94305, United States.*

[4]*SUNCAT Center for Interface Science and Catalysis, SLAC National Accelerator Laboratory, Menlo Park, CA 94025, United States.*

[5]*Department of Chemistry, Stanford University, Stanford, CA 94305, United States.*

[6]*Department of Materials Science and Engineering, Stanford University, Stanford, CA 94305, United States.*

[7]*Advanced Light Source, Lawrence Berkeley National Laboratory, 1 Cyclotron Rd. Berkeley, CA 94720, United States.*

[8]*Molecular Biophysics and Integrated Bioimaging Division, Lawrence Berkeley National Laboratory, 1 Cyclotron Rd. Berkeley, CA 94720, United States.*

[9]*Stanford Synchrotron Radiation Lightsource, SLAC National Accelerator Laboratory, Menlo Park, CA 94025, United States.*

[‖]*These authors contributed equally to this work.*

Corresponding Author

*E-mail: wsdrisdell@lbl.gov; chahn@slac.stanford.edu; jaramillo@stanford.edu; mehta@slac.stanford.edu; rydavis@slac.stanford.edu

Experimental Section

Synthesis of Cu thin film and electrochemical flow cell assembly

Polycrystalline Cu (hereafter, Cu(pc)) thin-films were synthesized via physical vapor deposition (PVD) inside a Temescal BJD-1800 evaporator as described in a previous report.[1] Cr layer (3 nm) was deposited on to n^+ Si(100) wafer for enhanced adhesion. 50 nm of Cu was then deposited onto the Cr adhesion layer. The Cu(pc) thin-films prepared from this method have been shown to exhibit a smooth surface with low roughness, which is suitable for grazing incidence (GI) geometry.[2] To confirm the purity and chemical state on the surface of the as-prepared Cu(pc) thin-films, X-ray photoelectron spectroscopy (XPS) spectra were collected using a PHI Versaprobe 1 XPS spectrometer at the Stanford Nanoscience Shared Facility (SNSF) with an incident Al Kα radiation of 1486 eV. Survey scans were acquired over a binding energy range of 0–1000 eV with a spot size of 100 μm and a resolution of approximately 1 eV.

The as-prepared Cu(pc) thin-film was mounted into a custom-made electrochemical flow cell that accommodates the GI geometry with controllable mass transport of reactants. Additional details about this cell are provided in a previous report.[3] Briefly, two platinum wires were stretched laterally ~ 200 μm above the surface of the Cu(pc) thin-film electrode and served as the counter electrode. The cell was connected to a Ag/AgCl reference electrode through a Luggin capillary. The assembled cell was connected to a flow system that consists of a gas sparging chamber and an HPLC pump (Scientific Systems, Inc.) to control the flow rate of electrolyte over the electrode surface. The electrolyte was prepared from buffer solutions of K_2HPO_4 (Fluka Analytical TraceSELECT >99.999% trace metals basis), KH_2PO_4 (Fluka Analytical TraceSELECT >99.995% trace metals basis), and $KHCO_3$ (Sigma-Aldrich, 99.95% trace metals basis). An electrolyte reservoir was continually sparged with CO_2 or Ar gas at a flow rate of 20 sccm controlled by a mass flow controller. A chelating agent (Chelex 100, Sigma-Aldrich) was added to the electrolyte reservoir to remove any metal impurities from the electrolyte. Using the HPLC pump, a thin layer (~ 500 um) of electrolyte flows over the surface of the Cu electrode at a flow rate of 45 mL/min, which corresponds to ~ 0.5 m/s linear velocity over the electrode surface. This high electrolyte flow rate and the presence of chelating agents can help to prevent redeposition on the working Cu electrode of any metal ions present in the

electrolyte or dissolved from the counter electrode. A BioLogic SP-300 potentiostat was used to control the working electrode potential.

Electrochemical CO_2 reduction selectivity and activity measurements

Cu(pc) thin-films were synthesized as described above and mounted in a custom-made two-compartment electrochemical cell, of similar design as described in a previous publication.[4] In brief, it consists of a Selemion membrane separating two compressed electrode compartments each filled with 8 mL of electrolyte. The electrolyte was 0.1 M $KHCO_3$ prepared by bubbling CO_2 into 0.1 M KOH (99.994%, Sigma-Aldrich). The exposed surface areas of the electrodes are 5.9 cm^2, with the as-deposited Cu(pc) thin-film serving as the working electrode and a Pt foil as the counter electrode. Prior to assembly, the polycarbonate cell parts were stored overnight in 0.1 M H_2SO_4, and the Pt foil counter was stored in concentrated nitric acid; all were rinsed with DI water and dried with N_2 gas for assembly. The reference electrode was a saturated KCl Ag/AgCl leakless reference electrode (LF-1.6-100, Innovative Instruments) calibrated versus a standard hydrogen electrode (SHE) before electrolysis. The Cu(pc) thin-film was tested with chronoamperometry (CA) at three sequential potentials (-0.635V, -0.856V, and -0.985V vs RHE), each for 1 hr. Prior to electrolysis, CO_2 gas was bubbled into both compartments at 20 sccm until electrolyte saturation, and flow was maintained during electrolysis; the effluent from the working electrode compartment was fed into a gas chromatographer (MG3, SRI). Gas and liquid products were quantified with gas chromatography and NMR spectroscopy, respectively. Reported gas product quantification was the average from three injections into the gas chromatographer, each done at 5, 23, and 41 minutes into the CA. For liquid product quantification, a 1 mL aliquot of electrolyte from the working electrode compartment was taken at the end of each CA to prepare NMR samples. Prior to the next CA measurement, 1 mL of fresh electrolyte was added to the working electrode compartment to maintain a constant volume. For NMR samples taken after CAs subsequent to the first CA, the diluted concentration of the products from the previous CAs is subtracted from the total concentration; hence, only the products generated in the latest CA will be accounted for during quantification.

In-situ grazing incidence X-ray absorption spectroscopy (GIXAS)

In-situ GIXAS measurements were performed at beamline 11-2 at the Stanford Synchrotron Radiation Lightsource (SSRL). The incident photon energy for Cu K-edge GIXAS measurements was controlled by a Si (220) double-crystal monochromator. Energy calibration was conducted using a 5 μm Cu reference foil, defining 8979 eV as the maximum of the first inflection point of the first derivative of the reference spectrum. Harmonic rejection and collimation of the beam were achieved with a Rh-coated silicon mirror set with a 15 keV cut-off. The beam was focused downstream of the monochromator with a toroidal silicon mirror and in-hutch slits to acquire a vertical focus of ~30 microns and a nominal spot width of 1 mm. Data were collected as fluorescence excitation spectra at room temperature using a Ge 100 element detector (Canberra) located at a 90° angle to the incident X-ray beam. Photon energy was resolved and integrated with XIA DXP-XMAP digital photon processors. The GIXAS data were collected at probe depths of 2.6 nm (incidence angle, $\alpha = 0.16°$), 3.8 nm ($\alpha = 0.24°$), 7.9 nm ($\alpha = 0.28°$), 84.7 nm ($\alpha = 0.35°$) and 2650 nm (bulk, $\alpha = 0.5°$).[5]

Data analysis of Cu K-edge X-ray absorption near-edge spectroscopy (XANES) and extended X-ray absorption fine structure (EXAFS) spectra were conducted using the Athena software package.[6] Pre-edge and post-edge backgrounds were subtracted from the XAS spectra, and the resulting spectra were normalized by edge height. For the XANES and EXAFS spectra, one or two points of glitches were corrected by using the deglitching process in the SamView program in the SIXpack software package.[7]

In-situ grazing incidence X-ray diffraction (GIXRD)

In-situ GIXRD measurements were conducted at SSRL on Beamline 2-1 using the same electrochemical cell and setup as the GIXAS. The incident X-ray energy was tuned to 17.0 keV (0.729 Å). A Huber 2-circle goniometer was employed to control the incidence angle of the X-rays. To reduce scattering from the Si substrate, a spot size with a 20-40 μm vertical height and 1 mm nominal width was chosen. Scattered X-rays were detected with a Pilatus 100K area detector from Dectris (487 x 195 pixels, 172 μm x 172 μm pixel size). GIXRD diffractograms were measured at probe depths of 2.6 nm (incidence angle, $\alpha = 0.15°$), 4.0 nm ($\alpha = 0.18°$), 14.0

nm (α = 0.20°), 35.8 nm (α = 0.22°), 83.4 nm (α = 0.3°) and 169.8 nm (bulk, α = 0.5°).[5]

The 1D diffractograms in the manuscript were derived from the collected 2D images by binning detector pixels according to 2θ and dividing by the incident beam intensity. The integration of 2D images into the 1D diffractograms was done using the EC_Xray python package, which has been developed for analyzing data collected with SSRL's SPEC program.[8] The resulting 1D diffractograms were corrected for refraction at the electrode-electrolyte interfaces using a modified version of Toney and Brennan's work.[3,9] The profile fitting for 1D diffractograms was performed using the Highscore program (Malvern PANalytical). Polynomial backgrounds were subtracted from the integrated diffractograms and a pseudo-Voigt function was used to fit the whole diffractogram. To estimate the errors in determining d-spacing, we used four different asymmetry functions for considering peak asymmetry (Split shape, Split width, Split width and shape, and Figer, Cox, Jephcot).

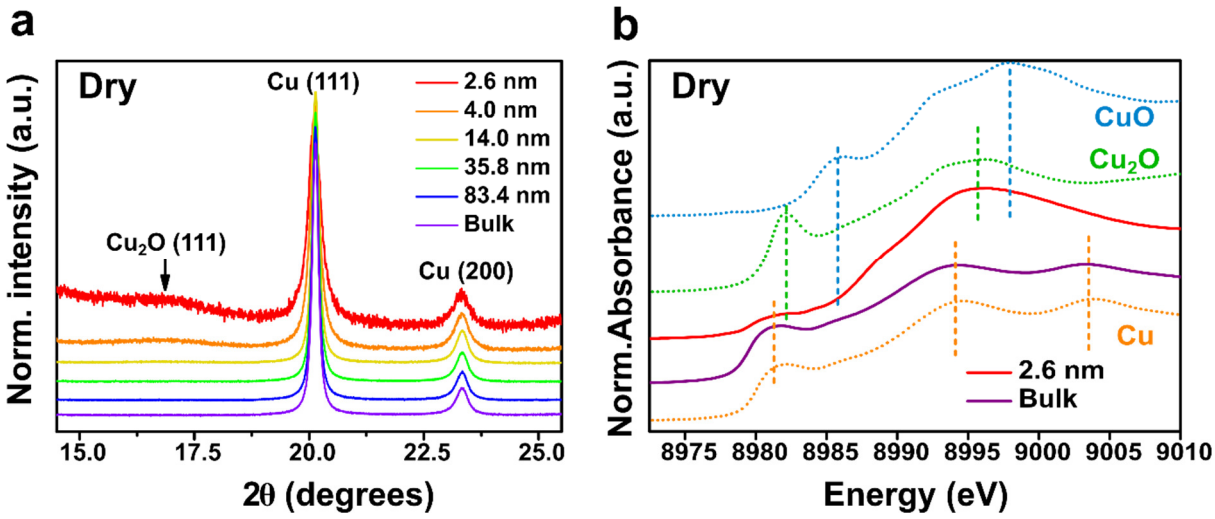

Figure S1. GIXRD and GIXAS of as-synthesized polycrystalline Cu electrode. (a) Diffractograms of as-synthesized Cu thin-film as a function of probe depth. The arrow indicates a broad $Cu_2O(111)$ peak only in the probe depth of 2.6 nm. (b) GIXAS spectra of as-synthesized Cu thin-film at near-surface (2.6 nm) and bulk (over 100 nm) with comparison to Cu (orange), Cu_2O (green), and CuO (blue) reference spectra (dotted lines). Vertical lines point out the major features of each reference spectrum for comparison.

After the 50 nm thick Cu(pc) films were mounted into the electrochemical flow cell, we collected both GIXRD and GIXAS data on the as-prepared Cu thin films at various incidence angles. The GIXRD pattern at a depth of 2.6 nm (~12 monolayers) shows that a faint peak centered at 16.9^{o} is observed, which is attributed to the disordered $Cu_2O(111)$ phase. The XANES spectrum at 2.6 nm probe depth exhibited a mixture of Cu_2O, CuO, and Cu, whereas only Cu was observed in the bulk. Thus, these results show that combined measurements can yield complementary information on the Cu surface, including oxidation states from the GIXAS as well as crystallographic structure from the GIXRD.

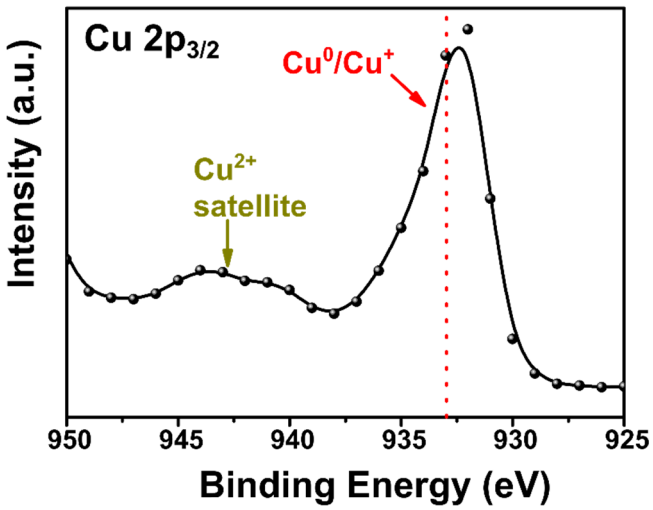

Figure S2. XPS of the Cu $2P_{3/2}$ core-level regions of as-prepared Cu thin-film. The surface oxidation states are consistent with the XANES spectrum at a probe depth of 2.6 nm, indicating a mixture of oxidation states in the surface oxide layer.

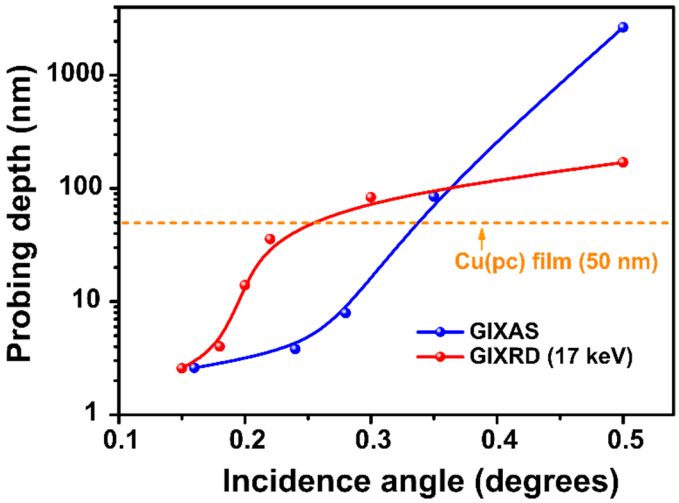

Figure S3. Calculated probe depths in the GIXAS and GIXRD as a function of incidence angles. In the case of GIXAS, the X-ray energy is scanned from 8750 eV to 9380 eV for XANES and 8750 eV to 9535 eV for EXAFS. We then select the largest probe depth during the XAS scans because the Cu(pc) thin film electrode is not perfectly smooth. In the case of GIXRD, fixed X-ray energy of 17 keV was used. The as-synthesized thin-film thickness of 50 nm is indicated by a dashed orange line for comparison.

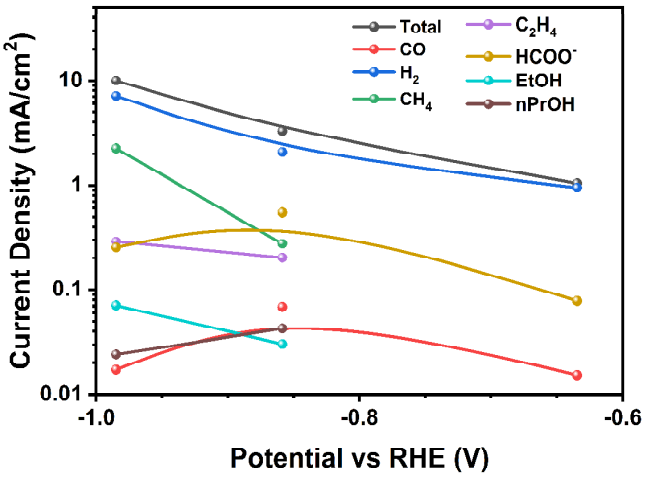

Figure S4. Electrochemical CO_2 reduction selectivity and activity trend. The partial current densities for all major CO_2RR products and the HER on Cu(pc) thin-film (50 nm) with a Cr (3 nm) adhesion layer on a Si substrate. The CO_2 reduction activity of Cu(pc) thin-films is similar to that of a Cu(pc) foil[4] and epitaxial Cu thin-films[1] tested with the same experimental methods and electrochemical cell design. It is known that polycrystalline Cu surfaces can restructure under CO_2R conditions with (111) and (100) facets,[10] with the dominating facet varying depending on experimental conditions and time-dependent evolution of the surface. A variety of minor products were also detected, including allyl alcohol, glycoaldehyde, acetate, and methanol, similar to what's detected from experiments on Cu(pc) foils.[4] In all, the CO_2R activity trends for the Cu(pc) thin-film clearly follow what is expected for Cu(pc) surfaces.

Notably, there is an HER activity enhancement beyond that expected for a typical Cu(pc) surface. We hypothesize that the Cr adhesion layer has a role in this enhancement as it is known to catalyze the HER under CO_2RR conditions. The Cr adhesion layer could be exposed through pinholes in the Cu(pc) thin-film, leading to high background HER activity from this layer or dissolution and redeposition of Cr when cycling between reductive potentials and open circuit. Also, Cr and Cu could interdiffuse during the PVD process through grain boundaries in the Cu(pc) thin-film. Such surface contamination is not likely to be detected with XPS as the activity of Cu surfaces is known to be sensitive even to submonolayer coverages of other transition metals.[11] Dissolution and redeposition, and diffusion, of chromium adhesion layers in electrochemical experiments has been described before, albeit with a gold thin-film electrode.[12]

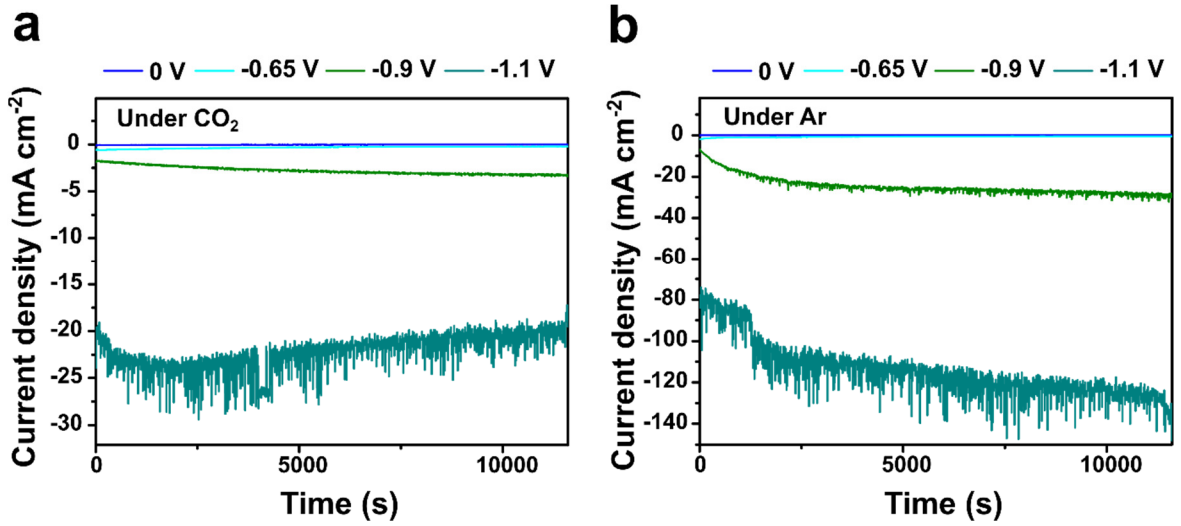

Figure S5. (a,b) Geometric current densities of a Cu(pc) thin-film as a function of the applied potentials under CO_2-purged 0.1 M $KHCO_3$ (pH ~6.8, a) and Ar-purged 0.1 M $K_xH_{3-x}PO_4$ electrolytes (pH ~6.8, b).

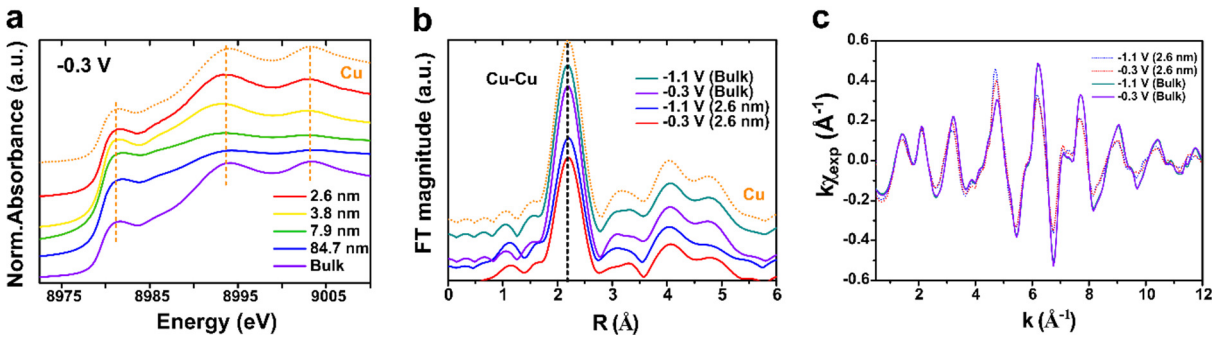

Figure S6. (a,b) XANES (a) and R-space EXAFS (b) spectra at -0.3 V vs. RHE as a function of probe depths and applied potentials. The Cu (orange) reference spectra (dotted line) are plotted for comparison. (c) *In-situ k*-space EXAFS (*k*-weighted) of Cu(pc) thin-film at a probe depth of 2.6 nm and bulk as a function of the applied potentials (-0.3 and -1.1 V). Strong damping of the EXAFS amplitude is observed for near-surface spectra (2.6 nm) due to the over-absorption effect.

The XANES spectra at -0.3 V as a function of probe depth showed distorted and dampened features, attributed to angle-dependent over-absorption.[3,13] Since the over-absorption only affects EXAFS amplitudes without changing its phase,[14] we confirm that the metallic Cu is the only phase through the whole thickness of the film.

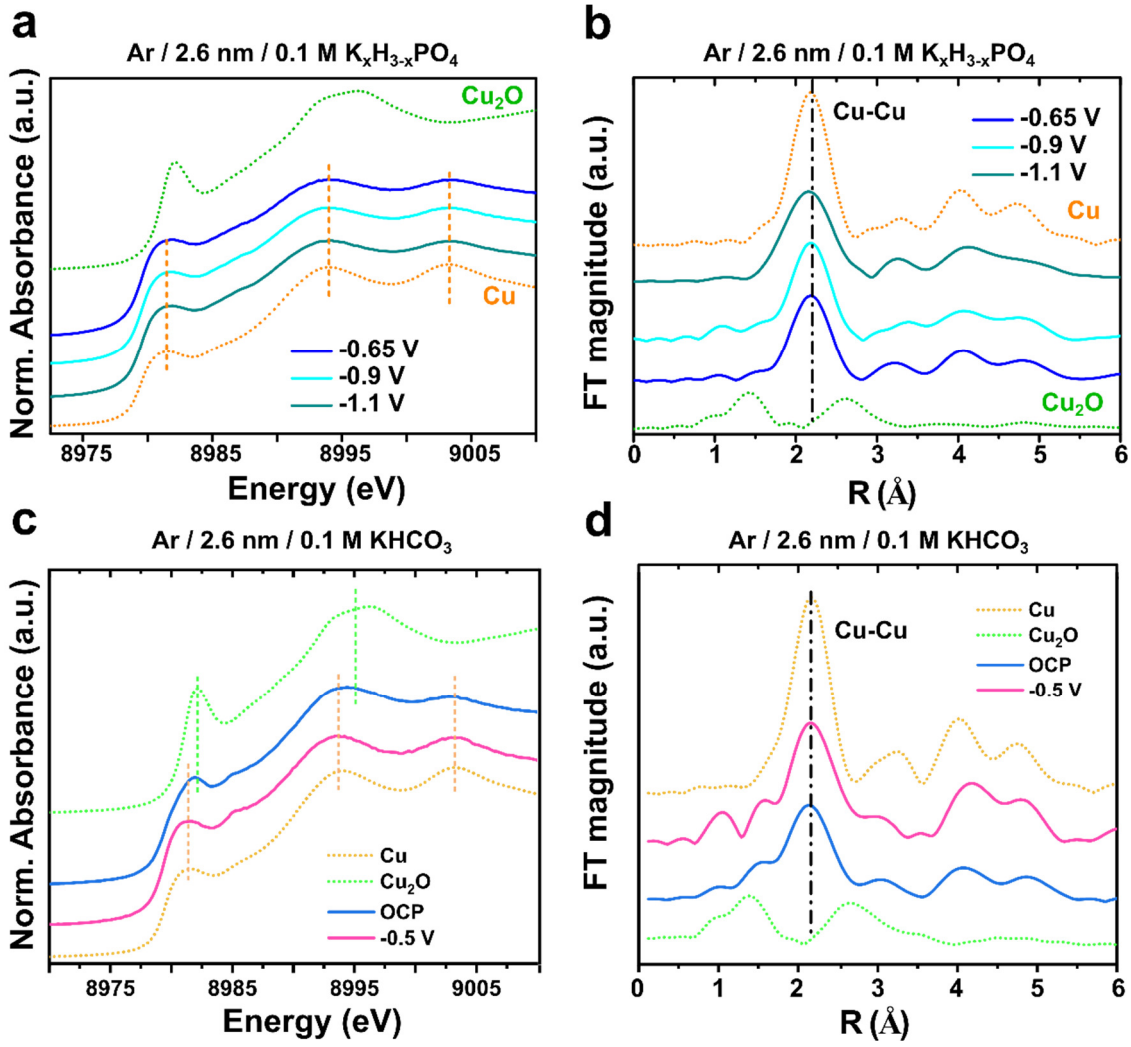

Figure S7. *In-situ* GIXAS of Cu(pc) thin-film electrode at a probe depth of 2.6 nm in Ar-saturated 0.1 M $K_xH_{3-x}PO_4$ (pH ~6.8, a and b) and 0.1 M $KHCO_3$ electrolyte (pH ~10, c and d). XANES (a and c) and Fourier-transformed EXAFS (b and d) spectra as a function of the applied potentials. The Cu (orange) and Cu_2O (green) reference spectra (dotted line) are plotted for comparison.

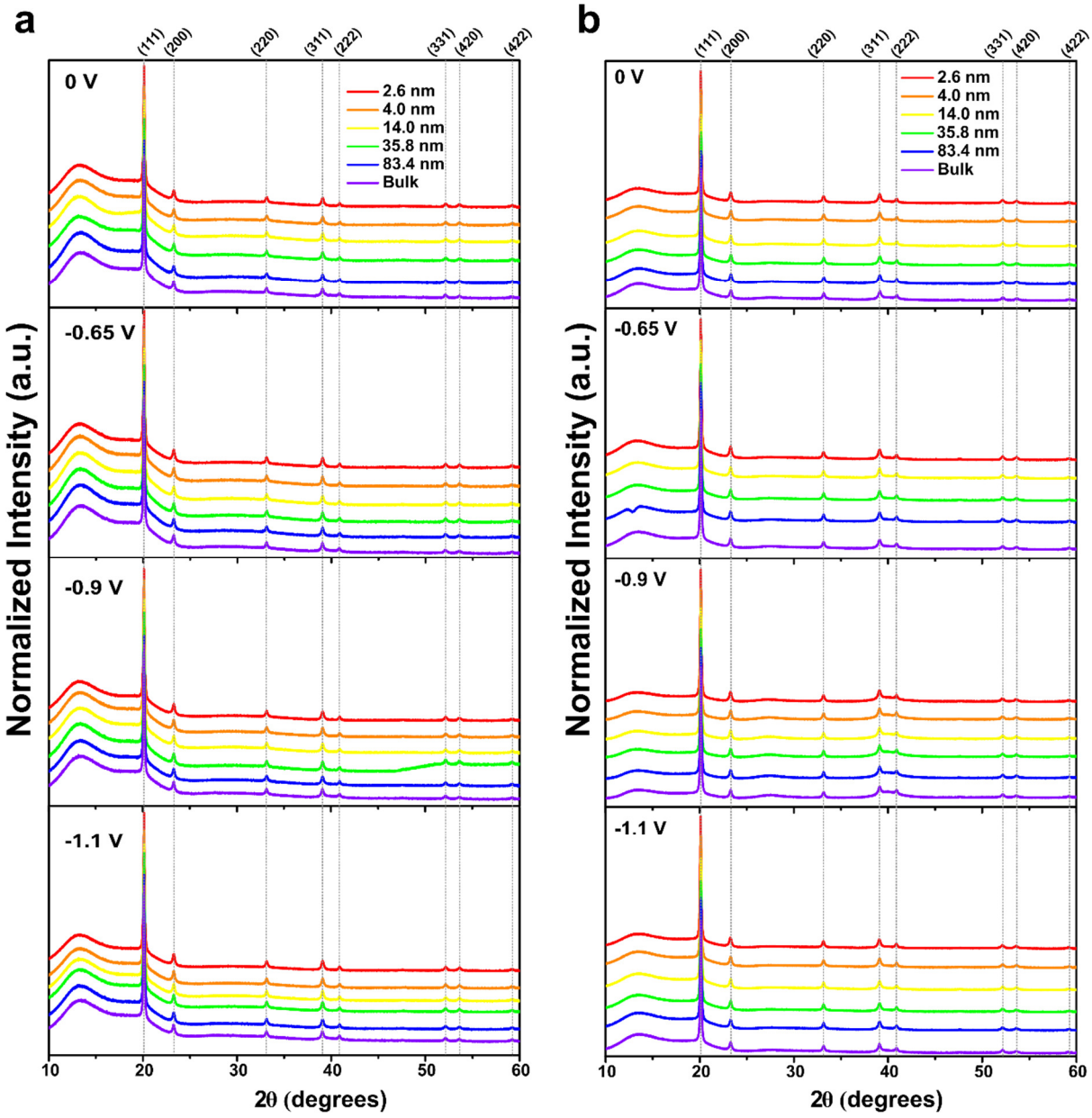

Figure S8. *In-situ* GIXRD diffractograms as a function of probe depth and applied potential in CO_2-purged 0.1 M $KHCO_3$ (pH ~6.8, a) and in Ar-purged 0.1 M $K_xH_{3-x}PO_4$ electrolytes (pH ~6.8, b). All the diffractograms were corrected for refraction at the electrode-electrolyte interface. The vertical lines indicate the calculated Bragg peaks of Cu for 17 keV X-rays.

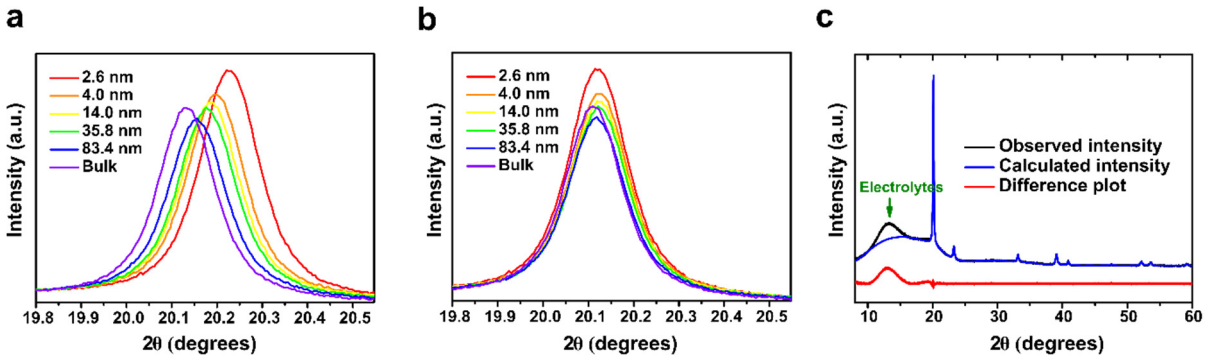

Figure S9. *In-situ* GIXRD at various probe depths (α = 0.15° (2.6 nm), α = 0.18° (4.0 nm), α = 0.20° (14.0 nm), α = 0.22° (35.8 nm), α = 0.30° (83.4 nm) and α = 0.5° (169.76 nm) of a Cu(pc) electrode at 0 V vs. RHE in CO_2-purged 0.1 M $KHCO_3$ (pH ~6.8) before (a) and after (b) refraction correction. The peak positions are shifted from the Bragg angles because incident X-rays are refracted at the electrolyte (liquid)—electrode (solid) interface. This refraction leads to a shift of 2θ toward a higher scattering angle and the refractive effects are largest at very small incidence angles. We correct for refraction using a modified version of Toney and Brennan's method which accounts for the liquid-solid interface.[9] After correcting for refraction, the (111) peak position aligns at all incidence angles after refraction correction except the bulk spectrum at incidence angle (α) of 0.5. One possibility that could account for this difference is a lower effective surface density in the thin film compared to the nominal density (8.9 g/cm^3).[15] Additionally, the polycrystalline Cu samples could have surface heterogeneities and broad distribution of domain sizes through the film. Since the refraction correction assumes homogeneously flat surfaces, the surface roughness and crystallite size distribution in the thin-film could contribute to this difference.[16] Therefore, we believe that a deviation between (111) d-spacing values of surface and bulk (~0.05%, Figure S12a) is a result of an artifact originating from the refraction correction process. (c) A GIXRD spectrum of a Cu(pc) thin-film at a probe depth of 2.6 nm in CO_2-purged 0.1 M $KHCO_3$ (pH ~6.8). The peaks were fitted with pseudo-Voigt function, except a very broad peak centered around 2θ = 13˚ originating from the scattering by the electrolyte. The difference plot between the measured and calculated spectra shows a mismatch in Cu(111) peak because profile analysis by the function does not consider asymmetric peak broadening.

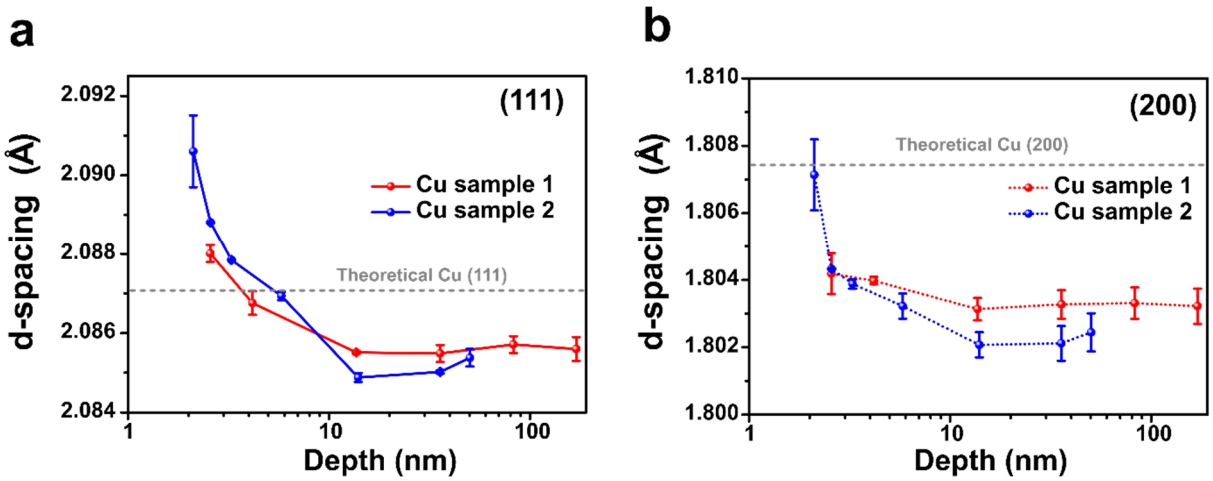

Figure S10. Error estimations for evaluating d-spacing. The calculated Cu(111) (a) and Cu(200) (b) d-spacing of the as-prepared Cu (pc) thin-film before connecting to the electrolyte flow system. The observed diffractograms were fitted by a pseudo-Voigt function that presumes all the diffraction peaks are symmetric. However, an asymmetric peak broadening can occur as a result of stacking faults, chemical variation in the sample, and a non-stoichiometric compound with a certain phase width. Since the peak asymmetry cannot be modeled with the conventional function used for peak profile analysis, we treated the peak asymmetry as an error source for estimation of d-spacing in Cu Bragg peaks. Moreover, the synthetic reproducibility of Cu(pc) thin-films can contribute a systemic error to the estimation of lattice parameters. Therefore, we considered these two error terms and calculated the error as ±0.001 Å in our experiments.

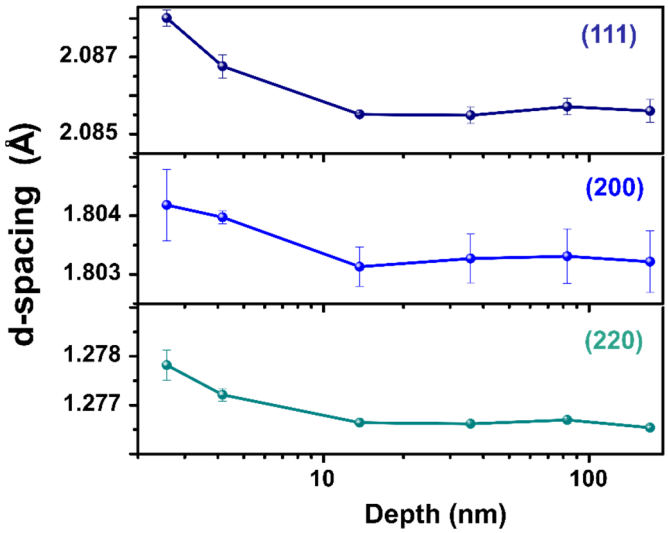

Figure S11. The calculated d-spacing of as-prepared Cu(pc) thin-film for Cu(111), (200), and (220) at a probe depth of 2.6 nm. The presence of the native oxide structure at the surface can cause a slight increase in d-spacing for Cu Bragg peaks, possibly attributable to the lattice mismatch between metallic Cu (3.615 Å) and Cu_2O (4.270 Å).

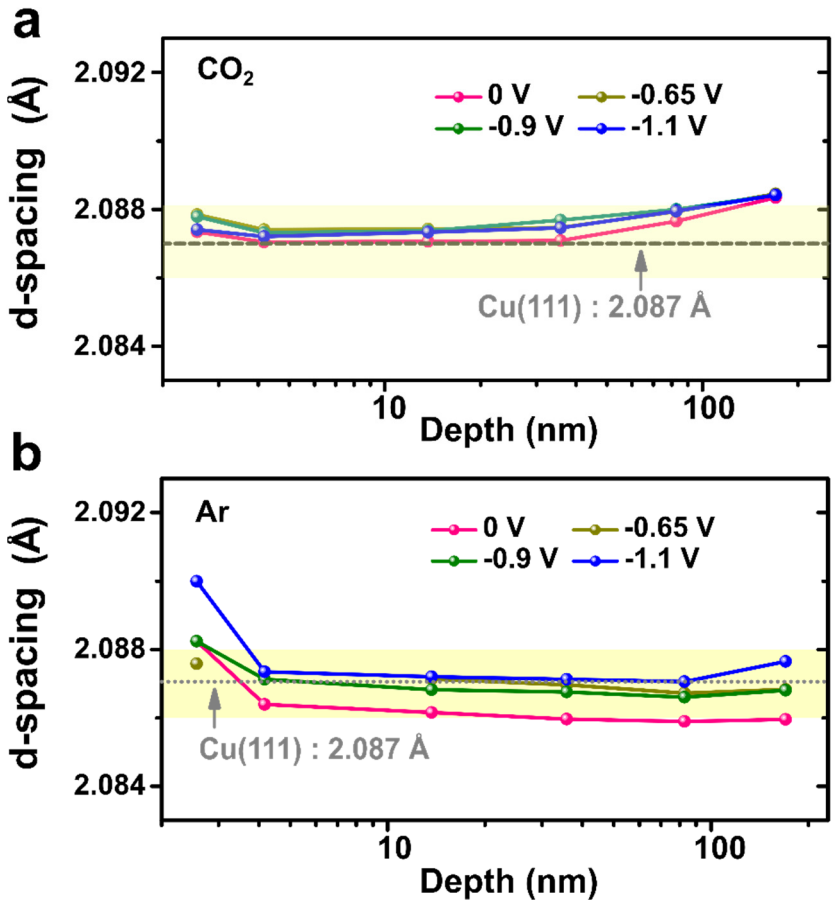

Figure S12. (a,b) The Cu(111) d-spacing values calculated from *in-situ* GIXRD of Cu(pc) thin-film electrode in CO_2-purged 0.1 M $KHCO_3$ (a) and Ar-purged 0.1 M $K_xH_{3-x}PO_4$ electrolytes (b) as a function of the applied potential. The theoretical d-spacing of Cu(111) (grey dashed line) and estimated error (yellow region) is indicated for comparison. The changes in d-spacing as a function of the applied potentials and probe depth are subtle and are within the estimated error range. In the Ar-purged electrolytes, a 0.14% expansion was observed only in the near-surface (2.6 nm) at -1.1 V, which may be attributable to hydrogen-induced lattice expansion.

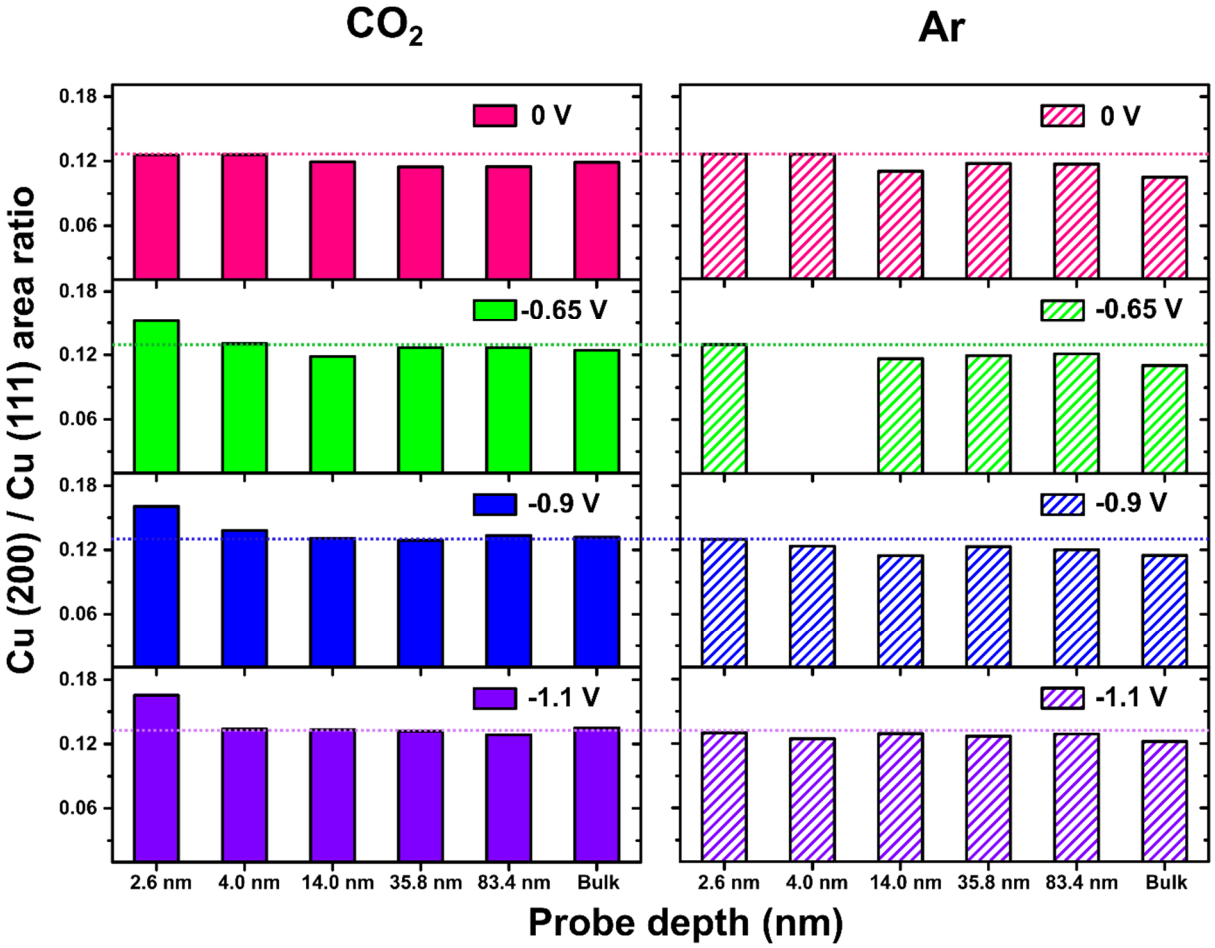

Figure S13. The integrated intensities (area) ratio of the Cu(200) to Cu(111) Bragg peak measured in the *in-situ* GIXRD as a function of the applied potential and probe depth in CO_2-purged 0.1 M $K_xH_{2-x}CO_3$ (pH ~6.8) and Ar-purged 0.1 M $K_xH_{3-x}PO_4$ (pH ~6.8) electrolytes. The horizontal dotted lines indicate the ratio values at a probe depth of 2.6 nm in the Ar-purged electrolyte for comparison.

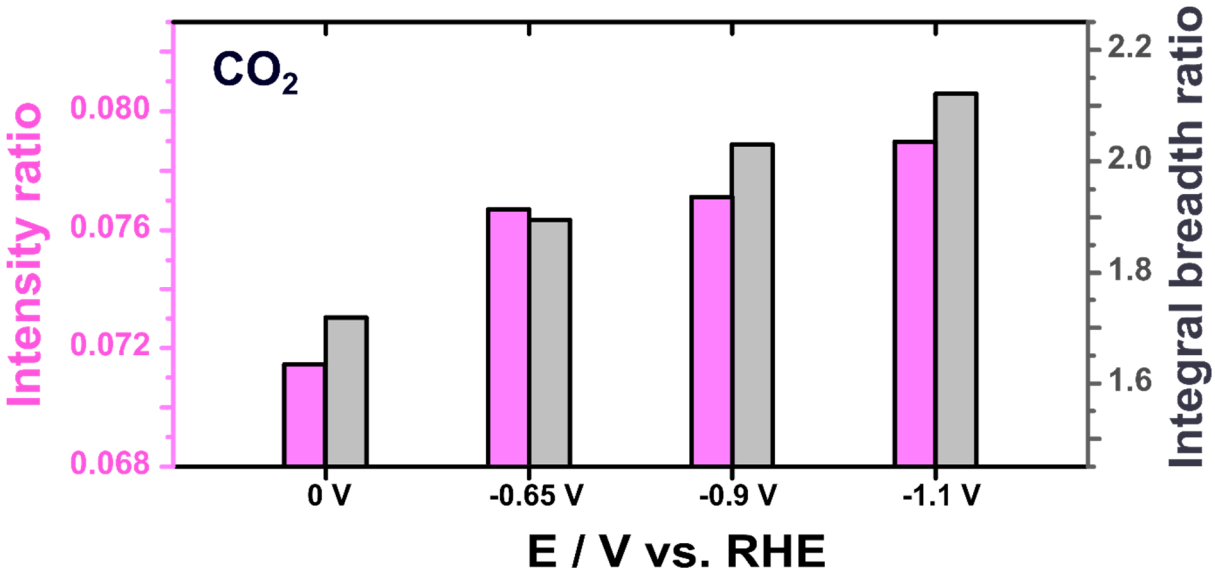

Figure S14. The intensity (peak height, pink) and integral breadth (peak width, grey) ratios of the Cu(200) to Cu(111) peak at a probe depth of 2.6 nm as a function of applied potential in the CO_2 electrolytes.

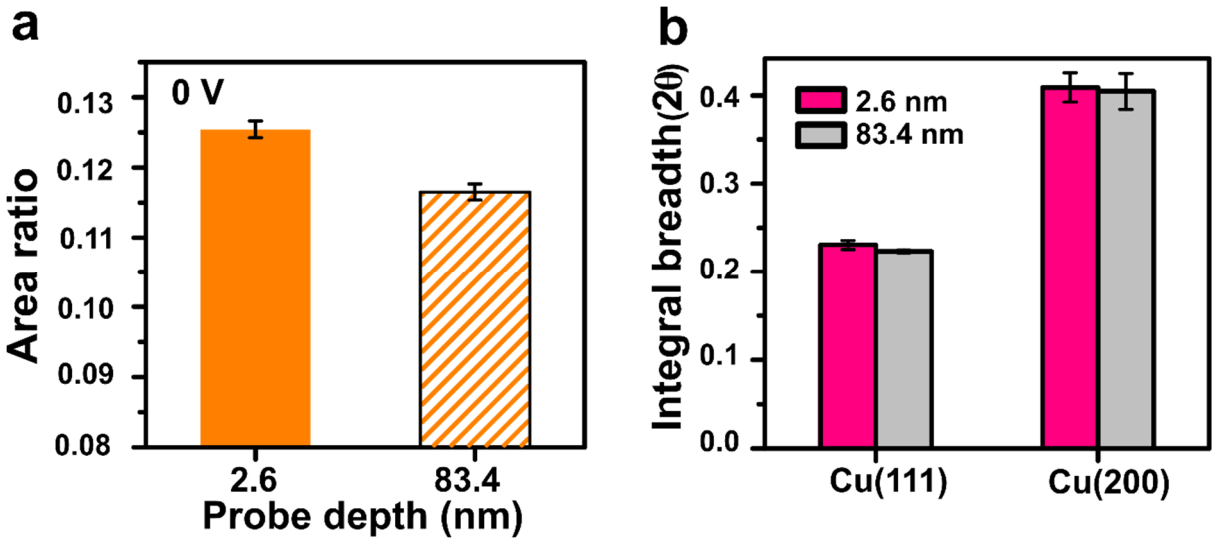

Figure S15. Error estimations for evaluating the ratio of Cu(200) to Cu(111) peaks at probe depths of 2.6 nm and 83.4 nm (a), and the integral breadth in Cu(111) and Cu(200) peaks at probe depths of 2.6 and 83.4 nm (b). The error bar represents the mean and standard deviations obtained from three different cases.

In the *in-situ* GIXRD experiments, the three samples investigated included 2 samples in CO_2-purged electrolyte and 1 sample in Ar-purged electrolyte. The onset potential of HER was previously observed at -0.3 V in N_2-purged 0.1 M $KHCO_3$,[17] and the onset potential of CO_2RR was previously observed at -0.65 V in CO_2-purged 0.1 M $KHCO_3$.[4] Thus, we assume that the Cu surface at 0 V does not undergo reconstruction in either the CO_2 or N_2-purged electrolytes (pH ~6.8 in both cases), resulting in a similar ratio in Figure 3. We consider the standard deviation of these three cases as the error for estimating area ratio and integral breadth.

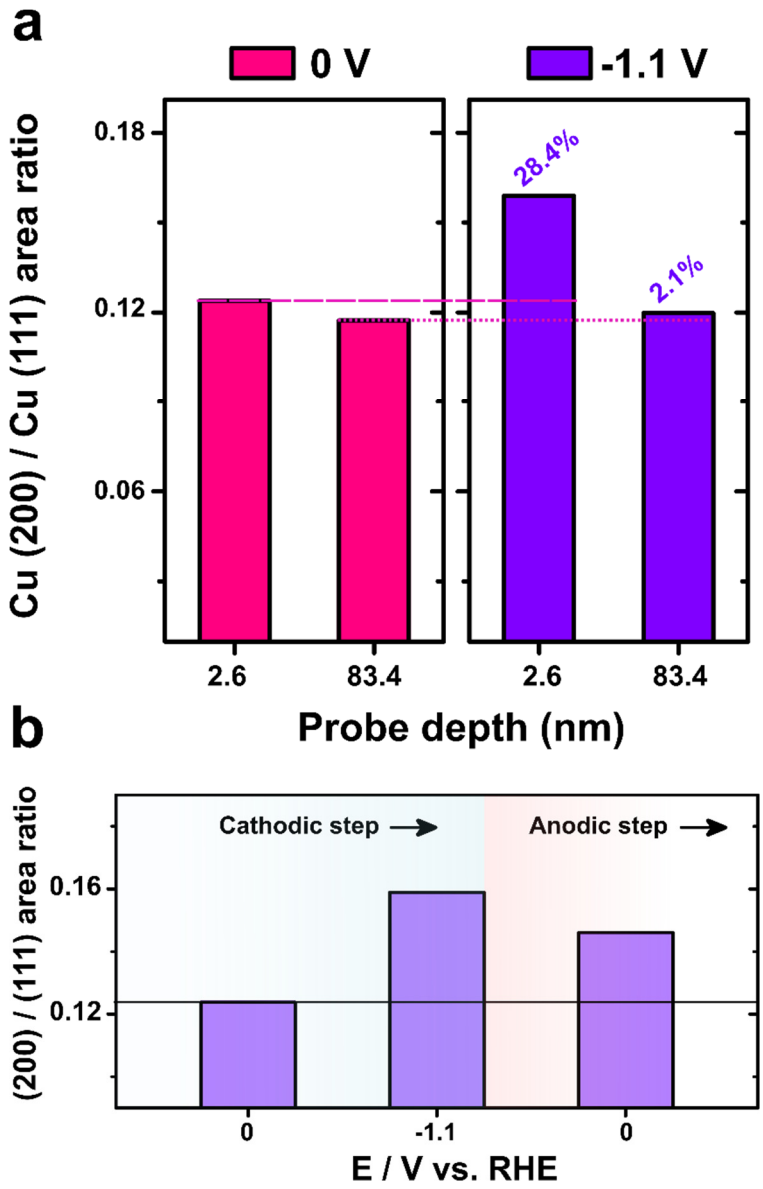

Figure S16. Reproducibility of the surface reconstruction from Cu(pc) to Cu(100)-like surface. The integrated intensity (area) ratio of Cu(200) to Cu(111) was measured from a different Cu(pc) sample. *In-situ* GIXRD was performed in the CO_2-purged 0.1 M $KHCO_3$ electrolyte as a function of probe depth (2.6 and 83.4 nm) and the applied potential (0 and -1.1 V). Each percentage above the bars indicates the increase of ratio compared to the value at 0 V. (b) Changes of (200)/(111) area ratio in cathodic and anodic steps at a probe depth of 2.6 nm.

Supplementary discussion

We note that our suggestion about adsorbed CO* intermediate-driven surface reconstruction is based on both theoretical calculations and experimental evidence that have been reported so far. Density functional theory (DFT) calculations of CO* adsorption indicate that CO* coverage dramatically increases while H* coverage starts to decrease sharply when the applied potential is more negative than -0.6 V vs. RHE.[18] Adsorbed CO* surface coverage can be as high as 0.52 monolayer under these conditions. These calculations correlate with spectroscopic observations of the Cu surface during the CO_2RR, demonstrating that the major intermediate species is CO* and the fractions of other intermediates, including COH*, CHO*, CCO*, and OCCOH*, are small and difficult to detect.[19,20] The *in-situ* attenuated total internal reflection Fourier-transform infrared (ATR-FTIR) spectroscopy measurements of Cu thin-films in CO- and CO_2-purged electrolytes showed similar CO adsorption peaks, demonstrating that CO adsorption and coverage are independent of how the CO* is produced.[21]

In our system, the different increase of Cu(200) / Cu(111) peak area in CO_2-purged and Ar-purged electrolyte elucidates that surface hydrogen and hydroxide species generated from HER have a limited effect on the surface reconstruction. We also observed a similar surface reconstruction in the same Cu(pc) thin-film under CO reduction conditions in CO-saturated 0.1 M KOH (pH ≈13) in a previous study.[8] In that study, the area ratio of Cu(200) / Cu(111) increased at -1.167 V vs. standard hydrogen electrode (SHE), which is a similar potential to that used in this study (-1.05 V vs. SHE). Considering that the local pH at the Cu surface increases up to 5 units in the H-cell[22] and ~2 units in the flow cell,[23] the catalytic environment under CO_2-purged 0.1 M $KHCO_3$ could be similar to the situation in CO-saturated 0.1 M KOH, leading to an assumption that adsorbed CO* is a key factor in the observed surface reconstruction. However, more rigorous experimental evaluation is needed to prove the assumption.

References

(1) Hahn, C.; Hatsukade, T.; Kim, Y.-G.; Vailionis, A.; Baricuatro, J. H.; Higgins, D. C.; Nitopi, S. A.; Soriaga, M. P.; Jaramillo, T. F., Engineering Cu surfaces for the electrocatalytic conversion of CO_2: Controlling selectivity toward oxygenates and hydrocarbons. *Proc.Natl. Acad. Sci. U. S. A.* **2017,** *114* (23), 5918-5923.

(2) Hahn, C.; Abram, D. N.; Hansen, H. A.; Hatsukade, T.; Jackson, A.; Johnson, N. C.; Hellstern, T. R.; Kuhl, K. P.; Cave, E. R.; Feaster, J. T.; Jaramillo, T. F., Synthesis of thin film AuPd alloys and their investigation for electrocatalytic CO_2 reduction. *J. Mater. Chem. A* **2015,** *3* (40), 20185-20194.

(3) Farmand, M.; Landers, A. T.; Lin, J. C.; Feaster, J. T.; Beeman, J. W.; Ye, Y.; Clark, E. L.; Higgins, D.; Yano, J.; Davis, R. C.; Mehta, A.; Jaramillo, T. F.; Hahn, C.; Drisdell, W. S., Electrochemical flow cell enabling operando probing of electrocatalyst surfaces by X-ray spectroscopy and diffraction. *Phys. Chem. Chem. Phys.* **2019,** *21* (10), 5402-5408.

(4) Kuhl, K. P.; Cave, E. R.; Abram, D. N.; Jaramillo, T. F., New Insights into the Electrochemical Reduction of Carbon Dioxide on Metallic Copper Surfaces. *Energy Environ. Sci.* **2012,** *5*, 7050.

(5) Henke, B. L.; Gullikson, E. M.; Davis, J. C., X-Ray Interactions: Photoabsorption, Scattering, Transmission, and Reflection at E = 50-30,000 eV, Z = 1-92. *Atom. Data Nucl. Data* **1993,** *54* (2), 181-342.

(6) Ravel, B.; Newville, M., ATHENA, ARTEMIS, HEPHAESTUS: data analysis for X-ray absorption spectroscopy using IFEFFIT. *J. Synchrotron Radiat.* **2005,** *12* (4), 537-541.

(7) Webb, S. M., SIXPack a Graphical User Interface for XAS Analysis Using IFEFFIT. *Phys. Scr.* **2005**, 1011.

(8) Scott, S. B.; Hogg, T. V.; Landers, A. T.; Maagaard, T.; Bertheussen, E.; Lin, J. C.; Davis, R. C.; Beeman, J. W.; Higgins, D.; Drisdell, W. S.; Hahn, C.; Mehta, A.; Seger, B.; Jaramillo, T. F.; Chorkendorff, I., Absence of Oxidized Phases in Cu under CO Reduction Conditions. *ACS Energy Lett.* **2019,** *4* (3), 803-804.

(9) Toney, M. F.; Brennan, S., Observation of the effect of refraction on x rays diffracted in a grazing-incidence asymmetric Bragg geometry. *Phys. Rev. B* **1989,** *39* (11), 7963-7966.

(10) Kim, Y-G.; Baricuatro, J.H.; Javier, A.; Gregoire, J.M.; Soriaga, M.P., The evolut ion of the polycrystalline copper surface, first to Cu(111) and then to Cu(100), at

a fixed CO2RR potential: A study by operando EC-STM. *Langmuir*. **2014,** *30,* 15053–15056.

(11) Clark, E. L.; Resasco, J.; Landers, A.; Lin, J.; Chung, L.-T.; Walton, A.; Hahn, C.; Jaramillo, T. F.; Bell, A. T., Standards and Protocols for Data Acquisition an d Reporting for Studies of the Electrochemical Reduction of Carbon Dioxide. *AC S Catalysis*. **2018,** *8*(7), 6560–6570.

(12) Hoogvliet, J. C.; Van Bennekom, W. P., Gold thin-film electrodes: An EQCM stu dy of the influence of chromium and titanium adhesion layers on the response. *E lectrochimica Acta*. **2001,** *47*(4), 599–611.

(13) Tröger, L.; Arvanitis, D.; Baberschke, K.; Michaelis, H.; Grimm, U.; Zschech, E., Full correction of the self-absorption in soft-fluorescence extended X-ray-absorption fine structure. *Phys. Rev. B* **1992,** *46* (6), 3283-3289.

(14) Booth, C. H.; Bridges, F., Improved Self Absorption Correction for Fluorescence Measurements of Extended X-Ray Absorption FineStructure. *Phys. Scr.* **2005**, 202.

(15) Lim, G.; Parrish, W.; Ortiz, C.; Bellotto, M.; Hart, M., Grazing incidence synchrotron x-ray diffraction method for analyzing thin films. *Mater. Res.* **1987,** *2* (4), 471-477.

(16) Scherzer, M.; Girgsdies, F.; Stotz, E.; Willinger, M.-G.; Frei, E.; Schlögl, R.; Pietsch, U.; Lunkenbein, T., Electrochemical Surface Oxidation of Copper Studied by in Situ Grazing Incidence X-ray Diffraction. *J. Phys. Chem. C* **2019,** *123* (21), 13253-13262.

(17) Kim, Y.-G.; Baricuatro, J. H.; Soriaga, M. P., Surface Reconstruction of Polycrystalline Cu Electrodes in Aqueous KHCO3 Electrolyte at Potentials in the Early Stages of CO2 Reduction. *Electrocatalysis* **2018,** *9* (4), 526-530.

(18) Luo, W.; Nie, X.; Janik, M. J.; Asthagiri, A., Facet Dependence of CO_2 Reduction Paths on Cu Electrodes. *ACS Catal.* **2016,** *6* (1), 219-229.

(19) Zhu, S.; Jiang, B.; Cai, W.-B.; Shao, M., Direct Observation on Reaction Intermediates and the Role of Bicarbonate Anions in CO_2 Electrochemical Reduction Reaction on Cu Surfaces. *J. Am. Chem. Soc.* **2017,** *139* (44), 15664-15667.

(20) Pérez-Gallent, E.; Figueiredo, M. C.; Calle-Vallejo, F.; Koper, M. T. M., Spectroscopic Observation of a Hydrogenated CO Dimer Intermediate During CO Reduction on Cu(100) Electrodes. *Angew. Chem. Int. Ed.* **2017,** *56* (13), 3621-3624.

(21) Gunathunge, C. M.; Li, X.; Li, J.; Hicks, R. P.; Ovalle, V. J.; Waegele, M. M., Spectroscopic Observation of Reversible Surface Reconstruction of Copper Electrodes under CO_2 Reduction. *J. Phys. Chem. C* **2017,** *121* (22), 12337-12344.

(22) Yang, K.; Kas, R.; Smith, W. A., In Situ Infrared Spectroscopy Reveals Persistent Alkalinity near Electrode Surfaces during CO_2 Electroreduction. *J. Am. Chem. Soc.* **2019,** *141* (40), 15891-15900.

(23) Lu, X.; Zhu, C.; Wu, Z.; Xuan, J.; Francisco, J. S.; Wang, H., In Situ Observation of the pH Gradient near the Gas Diffusion Electrode of CO_2 Reduction in Alkaline Electrolyte. *J. Am. Chem. Soc.* **2020,** *142* (36), 15438-15444.